Photocatalytic CO_2-Hydrogen Conversion via RWGSR over Ni/TiO_2 Nanocatalyst Dispersed in Layered MMT Nanoclay

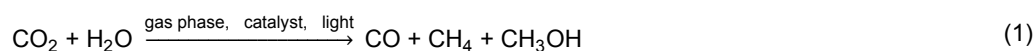Beenish Tahir, Muhammad Tahir*, Nor Aishah Saidina Amin

Chemical Reaction Engineering Group (CREG), Department of Chemical Engineering, Faculty of Chemical and Energy Engineering, Universiti Teknologi Malaysia (UTM), 81310 UTM Johor Bahru, Johor, Malaysia
mtahir@cheme.utm.my

The production of cleaner fuels from renewable and safer energy resources are highly demanding to mitigate energy crises and global warming. In this study, the use of cleaner photo-technology for selective and enhanced CO_2 reduction to fuels over nickel (Ni) modified titanium dioxide (TiO_2) dispersed in structured montmorillonite (MMT) nanoclay for photocatalytic CO_2-hydrogen conversion via reverse water gas shift (RWGS) reaction has been investigated. The catalyst samples, prepared by a single step sol-gel method, were characterised by XRD, FTIR, FESEM and UV–visible spectroscopy. XRD results revealed reduced in TiO_2 crystallite size with Ni and MMT loading and produced anatase phase of TiO_2. MMT is found efficient for the enhanced dispersion of TiO_2 while Ni-promoted efficient charges separation with hindered recombination rate over the structured MMT/TiO_2 nanocomposite. The photoactivity of Ni/TiO_2-MMT composite for CO_2 reduction was conducted in a continuous flow photoreactor using hydrogen as the reducing agent. The main products detected were CO and CH_4 with appreciable amounts of C_2H_4, C_2H_6 and C_3H_6 hydrocarbons. The maximum yield of CO produced as the main product over 3 wt% Ni-10 wt% MMT/TiO_2 catalyst was 9,429 µmole/g-cat, 209-fold higher than the amount of CO detected over the pure TiO_2. Evidently, Ni-promoted TiO_2 photocatalytic activity, while MMT is favourable for improved dispersion of Ni/TiO_2 catalyst. The dynamic and selective CO evolution was evidently due to efficient light distribution, enlarged active surface area and efficient charges separation with their hindered recombination rate by Ni and MMT. The stability of Ni/TiO_2 dispersed over MMT sustained over the irradiation time. With the use of green nanocomposite catalyst, CO_2 can be efficiently converted to cleaner fuels with all sustainable systems.

1. Introduction

Global warming caused by the drastic release of carbon dioxide (CO_2) induced by combustion of fossil fuels has drawn considerable attention to the need to address environmental challenges related to climate change (Ye et al., 2015). Among the other alternative methods for CO_2 mitigations, photocatalytic water splitting (Reverberi et al., 2016) and CO_2 reduction to fuels using light irradiation provides pathways toward economical and cleaner process (Low et al., 2017). Pioneered work on photocatalytic CO_2 reduction was conducted for the first time in 1979 and the products detected were CH_3OH, HCOOH, HCHO, CH_3COOH and CH_4 over semiconductors TiO_2, ZnO, WO_3, CdS and SiC (Inoue et al., 1979). During the past three decades, excessive efforts have been established to maximise activity, and selectivity of many semiconductors using different reducing agent, photo-catalysts and photo-reactors.

In the field of photocatalytic CO_2 reduction, the most of work has been related to using water as a reducing agent. Thermodynamically, H_2O is hardly reducible and CO_2 reduction with H_2O yielded lower amounts of products while selectivity is dependent on photo-catalysts and reaction system as discussed in Eq(1) and Eq(2) (Tahir et al., 2017a).

$$CO_2 + H_2O \xrightarrow{\text{gas phase, catalyst, light}} CO + CH_4 + CH_3OH \qquad (1)$$

$$CO_2 + H_2O \xrightarrow{\text{slurry system, catalyst, light}} CH_3OH + HCOOH + HCHO \tag{2}$$

Recently, hydrogen (H_2) is reported as an efficient reductant to maximise CO_2 reduction efficiency and products selectivity through reverse water gas shift (RWGS) reaction and CO_2-methanation reaction as explained in Eq(3) and Eq(4). Photocatalytic CO_2 reduction to CO by H_2 over Ag/TiO$_2$ NWs (Tahir et al., 2017d), has been reported with improved yield rate and selectivity. Photocatalytic RWGS CO_2 reduction could be a potentially workable to produce cleaner fuels with higher yield and selectivity.

$$CO_2 + H_2 \xrightarrow{\text{RWGS, catalyst, light}} CO + H_2O \tag{3}$$

$$CO_2 + H_2 \xrightarrow{\text{Methanation, catalyst, light}} CH_4 + H_2O \tag{4}$$

Titanium dioxide (TiO_2) as a semiconductor has attracted many researchers due to its numerous rewards such as relatively low price, non-toxic, excessive available, resistant to chemicals, and relatively high oxidative potentials (Kim et al., 2017). Conversely, photocatalytic efficiency of the pure TiO_2 is low due fast photo-generated charges recombination rate.

Surface modification of TiO_2 structure with electron acceptors using metals such as Au, Ag, Cu, Pt, Ce and La is a proven strategy to improve efficiency (Ali et al., 2017). Among the metals, Ni is attracting much attention due to appropriate fermi levels to transfer electrons from TiO_2 to metal co-catalyst, low cost and abundantly available. Ni/TiO2 activity can further be enhanced by their dispersion into the green clay structures. Using nanoclay as a support in which Ni/TiO$_2$ can be distributed on the surface of a suitable matrix, an efficient hetero-junction is produced. The other numerous benefits of natural clay materials are low cost, green materials and have high CO_2 adsorption capacity.

The most widely used clay mineral is montmorillonite (MMT) which is a multilayered nanoclay consists of octahedral sheet sandwiched between two silica tetrahedral sheets (Mulewa et al., 2017). This distinctive structure of MMT makes it suitable for high dispersion, enhanced sorption capacity and excellent charge trapping ability. Previously, the use of TiO_2/MMT in photocatalytic CO_2 reduction applications has been successfully investigated (Tahir et al., 2017c). It is obvious from the literature that MMT is the most widely studied clay for the growth of TiO_2 nanoparticles. In this context, further research involving photocatalytic RWGS reaction over MMT supported Ni/TiO$_2$ nanocatalyst for gas phase systems in a continuous monolith photoreactor to produce renewable fuels is warranted.

In this work, the use of Ni and MMT-clay to modify TiO_2 structure for photocatalytic CO_2 reduction via RWGS reaction in a continuous flow photoreactor has been investigated. The catalysts were synthesized by a modified sol-gel method and were characterized by XRD, FE-SEM, FTIR and UV-Vis spectroscopy. The role of Ni and MMT on the yield rate and products selectivity are critically discussed. In addition, the photocatalytic reaction mechanism for CO_2 reduction to CO via RWGS reaction was considered based on the experimental results.

2. Experimental

2.1 Catalyst preparation

The Ni/TiO$_2$ dispersed over MMT nanoclay was synthesized through a direct and single step sol-gel method using Tetra-isopropyl orthotitanate (98 %, Merck) and MMT (1.4P, Aldrich). Typically, 10 mL titanium solution (Tetra-isopropyl orthotitanate (98 %, Merck) dispersed in 30 mL isopropanol was taken into flask for the hydrolysis process. Next, the solution was hydrolysed by adding 7 mL acetic acid (1 M) diluted in 10 mL isopropanol under vigorous stirring. The mixture was stirred for another 24 h to get clear titanium sol. The solutions of nickel nitrate and montmorillonite (MMT (1.4P, Aldrich) dispersed in isopropanol were added into titanium sol. The process of stirring was continued for another 6 h until the thick sol was obtained. The sol obtained was transferred into a glass container for the monolith coating. The cordierite ceramic monoliths with square channels were dipped into the sol. Any excess soil was blown off using hot compressed air. The coating procedure was repeated to ensure constant loading. The coated monoliths were dried at 80 °C for 12 h before calcined at 500 °C for 5 h. Catalyst loading was calculated by subtracting the coated monolith weight from the initial bare monolith weight.

2.2 Characterization

The crystalline phase was investigated using powder X-ray diffraction (XRD; Bruker D8 advance diffractometer, 40 kV and 40 mA) with Cu- Kα radiation (λ = 1.54 A°). The infrared spectra were measured at room temperature in the range of 4,000 to 400 cm^{-1} with Spectrum 2000 Explorer Fourier Transformed

Infrared (FT-IR) Spectrometer. The scanning electron microscopy (SEM) was carried out with JEOL JSM6390 LV SEM instrument. UV-Vis diffuse reflectance absorbance spectra were determined using UV-vis spectrophotometer (Agilent, Cary 100) equipped with an integrated sphere. Fourier transform infrared (FTIR) spectroscopy was performed using Thermo Nicolet Avatar 360 FTIR spectrometer.

2.3 Photoactivity test

The reactor consists of stainless steel cylindrical vessel equipped with glass window of thickness 8 mm for passing out light irradiation. The catalyst coated monoliths with loading amount ~0.50 g was introduced inside the cylindrical stainless-steel chamber. The light source was a 200 W Hg lamp.

Prior to feeding, the reactor chamber was purged using purified helium (He) flow, then a mixture of gases (CO_2, H_2 and He) was constantly streamed through the reactor for 1 h to saturate the catalyst. The temperature inside the reactor was maintained at 100 °C using temperature controller. The gas mixture feed flow rate of 20 mL/min and CO_2/H_2 feed ratio of 1.0 was used in all the experiments. The products were analysed using an on-line gas chromatograph (GC-Agilent Technologies 6890 N, USA) equipped with thermal conductivity detector (TCD) and flame ionized detector (FID).

3. Results and discussion

3.1 Catalyst characterization

Figure 1a shows XRD patterns of TiO_2, MMT and Ni/MMT-loaded TiO_2 nanocomposite samples. XRD patterns of TiO_2 nanoparticles (NPs) revealed pure anatase and crystalline phase structure. Similarly, XRD pattern of MMT reflects broad basal of (0 0 1) located at $2\theta = 3.70°$, due to plate-shaped particles and stacking disorder of MMT layers. The XRD patterns of TiO_2 dispersed in MMT persisted its original reflection with no additional peaked appeared. However, all the TiO_2 peaks in MMT/TiO_2 sample become broader and weaker, and prominent MMT peak (0 0 1) disappeared. This has confirmed that MMT layered structure has disordered with uniform dispersion of TiO_2 NPs. With Ni loading to MMT/TiO_2, XRD patterns of TiO_2 NPs and MMT/TiO_2 composites persisted, while peaks of nickel in oxide or metal state were not detected due to its lower contents or its uniform dispersion in composite samples.

Figure 1b shows Infrared spectra of TiO_2, MMT and Ni-MMT/TiO_2 samples. The stretching bend at 1,616 cm^{-1} in the spectrum of pure TiO_2, shows chemisorbed H_2O is negligible. The MMT spectrum presents broadband at around 3,633 cm^{-2} attributed to Al_2OH group of octahedral layer, while the bands at around 1,616 cm^{-1} can be allocated to -OH and stretching and bending vibration of water molecules. The peak at 1,049 cm^{-1} corresponds to a symmetric vibration of SiO_2 tetrahedra while several peaks between 1,000 and 500 cm^{-1} can be attributed to Al-IV tetrahedra. The peaks between 1,000 and 500 cm^{-1} were assigned to bending vibration of Si-O. On the other hand, MMT/TiO_2 and Ni-MMT/TiO_2 samples show similar patterns as like TiO_2. The stretching band at about 1,049 cm^{-1} and very weak stretching at 450 to 550 cm^{-1} were observed due to the asymmetric stretching vibration of SiO_2 tetrahedra.
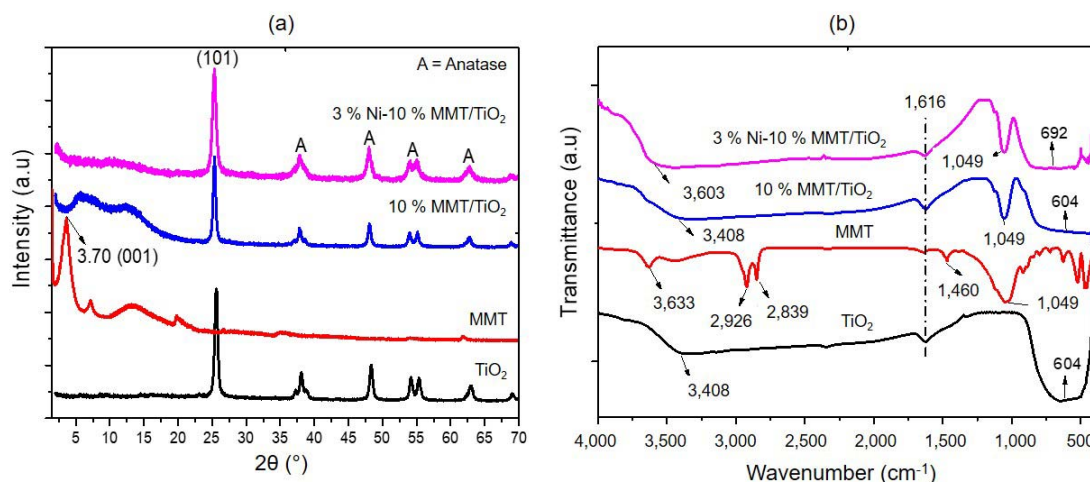

Figure 1: (a) XRD analysis and (b) FTIR analysis of TiO_2, MMT and Ni/MMT loaded TiO_2 samples

The structure and morphology of TiO_2, Ni/MMT-loaded TiO_2 samples is presented in Figure 2. SEM in Figure 2a shows MMT sheets stacked together. The uniform, spherical in shape and mesoporous TiO_2 nano-particles

are obvious in Figure 2b. Figure 2c illustrates SEM images of MMT/TiO$_2$ composite structure. Evidently, MMT layers are completely destroyed and TiO$_2$ NPs are well distributed with MMT, confirming efficient intercalation process, thus producing delaminated MMT/TiO$_2$ nanocomposite.

The addition of Ni into MMT/TiO$_2$ composite samples shows similar morphology as like MMT/TiO$_2$ but with more obvious TiO$_2$ NPs. This revealed successful development of Ni/TiO$_2$ NPs dispersed in MMT to produce Ni-MMT/TiO$_2$ composite sample.
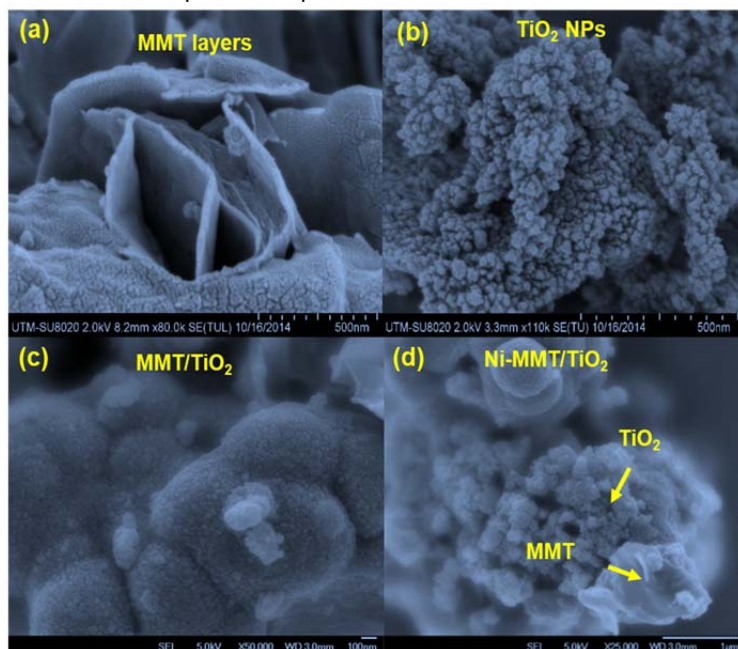

Figure 2: FESEM analysis of MMT and Ni/MMT-loaded TiO$_2$ nanoparticles. SEM images of (a) MMT layers, (b) TiO$_2$ NPs, (c) MMT-loaded TiO$_2$ NPs, and (d) Ni/MMT-loaded TiO$_2$ NPs

The UV–Vis diffuse reflectance absorbance spectra of the TiO$_2$, MMT/TiO$_2$ and Ni-MMT/TiO$_2$ samples are presented in Figure 3. Adding MMT into TiO$_2$, there was no significant effect on the absorption spectra, however, it was gradually shifted towards visible region with Ni-loading. The band gap of the samples was calculated according to plot of *(αhν)^2 vs photon energy (eV)*. The band gap energy of 3.11 and 3.10 eV obtained for TiO$_2$ and MMT/TiO$_2$ samples. However, the TiO$_2$ band gap energy was further reduced to 3.05 eV in Ni-loading MMT/TiO$_2$ samples. It is obvious that there is a gradual decrease in the band gap energy in Ni-loading TiO$_2$ samples compared to pure TiO$_2$ NPs.
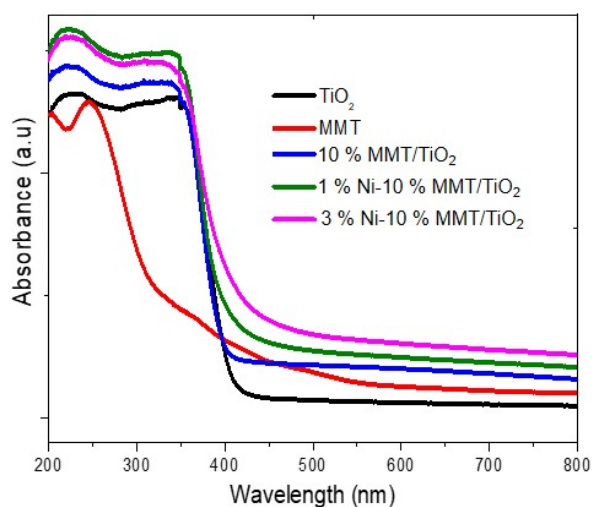

Figure 3: Diffuse reflectance absorbance spectra of TiO$_2$ NPs, MMT and Ni/MMT-loaded TiO$_2$ samples

3.2 Photocatalytic CO_2 reduction with H_2

Firstly, control experiments for photocatalytic CO_2 reduction with H_2 were conducted in the presence of photo-catalysts. Using all types of catalysts, carbon-containing compounds were not detected in the reaction system without reactants or light irradiations. Any carbon-containing compounds produced were derived from CO_2 photo-reduction only.

The effect of MMT-loading onto the catalytic activity of TiO_2 for photocatalytic CO_2 reduction to CO and CH_4 in the presence of H_2 as reducing agent at temperature 100 °C, irradiation time 2 h and CO_2/H_2 feed ratio 1.0 is presented in Figure 4a. Using all types of catalyst samples, CO was detected as the main product which was apparently due to RWGS reaction of CO_2 reduction with H_2. The pure TiO_2 has low photoactivity which gradually increased in MMT supported TiO_2 samples. Similarly, MMT/TiO_2 composite also promoted the production of CH_4. This was evidently due to efficient charge transfer, higher surface area and efficient CO_2 adsorption in MMT/TiO_2 samples. The optimal 10 wt% MMT/ TiO_2 sample was the most active over which the highest amount of CO and CH_4 were produced. Figure 4b shows the effect of irradiation time and Ni-loading on continuous production of CO during RWGS reaction of CO_2 with H_2 at CO_2/H_2 feed ratio 1.0, 100 °C and feed flow rate 20 mL/min. Initially, production of CO was much significant and then gradually reached to steady state in Ni-loaded MMT/TiO_2 samples. This significantly higher yield of CO in Ni-MMT/TiO_2 composite catalyst was due to efficient RWSG reaction in Eq(3), hindered charges recombination rate by Ni and efficient light distribution inside monolith photoreactor.
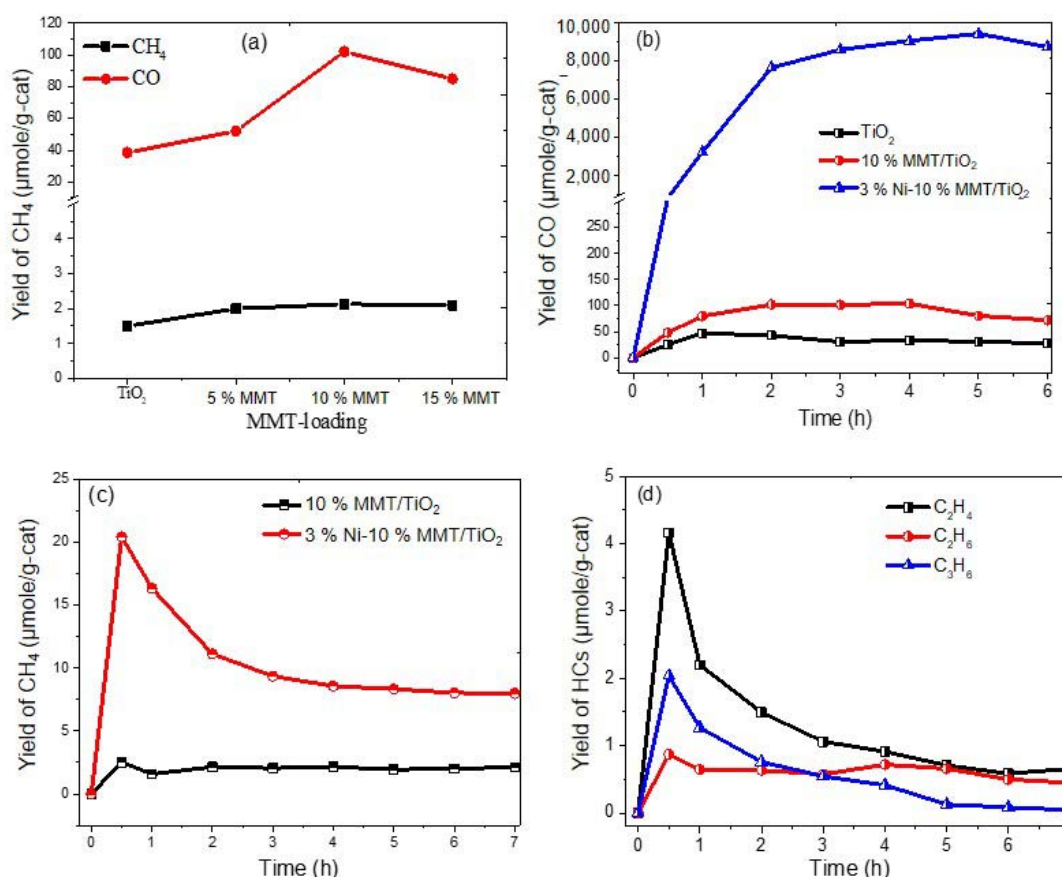

Figure 4: (a) Effect of MMT-loading on TiO_2 for CO and CH_4 production, (b) Effect of Ni-loading on the activity of MMT/TiO_2 samples for selective CO production, (c) CH_4 production over Ni-MMT/TiO_2 samples, (d) Production of C_2-C_3 hydrocarbons over Ni-MMT/TiO_2 composite catalyst

The highest reaction rate of CO over 3 wt% Ni-10 wt% MMT/TiO_2 was 2,268 µmole g-cat^{-1} h^{-1}, while it was only 26 and 8.5 µmole g-cat^{-1} h^{-1} over 10 % MMT/TiO_2 and TiO_2 NPs, respectively. These results show that CO_2 can efficiently and continuously be converted to cleaner fuels using Ni/TiO_2 dispersed in MMT nanoclay.

$$CH_4 + 2O_2 \xrightarrow{h\nu} CO_2 + 2H_2O \qquad (5)$$

$$C_2H_4 + 3O_2 \overset{h\nu}{\to} 2CO_2 + 2H_2O \qquad\qquad (6)$$

Figure 4c depicts the production of CH_4, in which CH_4 was produced in appreciable amount with $Ni-MMT/TiO_2$ catalyst. Similarly, production of higher hydrocarbons over $Ni-MMT/TiO_2$ is presented in Figure 4d. Among the hydrocarbons, C_2H_4 is detected in more quantity than C_2H_6 and C_3H_6 while their productions were decreased over the irradiation time. The decreased in hydrocarbons production was perhaps due to their oxidation as explained in Eq(5) and Eq(6). The CO_2 can efficiently be converted to CO and hydrocarbons using Ni as active metal and MMT as green clay materials in a continuous flow photoreactor system. The performance of $Ni-MMT/TiO_2$ catalyst was further compared with the reported values in literature. The amount of CO of 5.19 μmole g-cat^{-1} h^{-1} over g-C_3N_4/Bi_2WO_6 (Li et al., 2015), CO of 289.30 over 3 % Fe-10 % MMT/TiO_2 (Tahir et al., 2017b), a CO production of 1.91 μmole g-cat^{-1} h^{-1} was obtained over V-W-loaded TiO_2 in monolith photoreactor (Xiong et al., 2017) and Ag/TiO_2 NWs with CO production of 983 μmole g-cat^{-1} h^{-1} (Tahir et al., 2017b). The significantly enhanced performance of $Ni-MMT/TiO_2$ composite catalysts due to synergistic effect of Ni and MMT in a monolith photoreactor, resulting in enhanced activity and selectivity.

4. Conclusions

Photocatalytic CO_2 reduction to CO via RWGS reaction over Ni/TiO_2 nanocatalyst dispersed in MMT layered nanoclay has been successfully investigated. The yield rate of CO_2 reduction was increased significantly by introducing Ni in MMT/TiO_2 composite sample. Nickel is found to be very efficient for preventing charges recombination rate while MMT promoted Ni/TiO_2 dispersion with enhanced CO_2 adsorption. Monolithic support promoted efficient light distribution resulting in selective production of fuels. The finding of this study can be explored further for the production of other chemicals and fuels under solar energy irradiation.

References

Ali K.A., Abdullah A.Z., Mohamed A.R., 2017, Visible light responsive TiO_2 nanoparticles modified using Ceand La for photocatalytic reduction of CO_2: Effect of Ce dopant content, Applied Catalysis A, General, 537, 111-120.

Inoue T., Akira F., Satoshi K., Kenichi H., 1979. Photoelectrocatalytic reduction of carbon dioxide in aqueous suspensions of semiconductor powders, Nature, 277, 637-638.

Kim H.R., Razzaq A., Grimes C.A., 2017, Heterojunction p-n-p Cu_2O/S-TiO_2/CuO: Synthesis and application to photocatalytic conversion of CO_2 to methane, Journal of CO_2 Utilization, 20, 91-96.

Li M., Zhang L., Fan X., Zhou Y., Wu M., Shi J., 2015, Highly selective CO_2 photoreduction to CO over g-C_3N_4/Bi_2WO_6 composites under visible light, Journal of Materials Chemistry A, 3, 5189-5196.

Low J., Cheng B., Yu J., 2017, Surface modification and enhanced photocatalytic CO_2 reduction performance of TiO_2: a review, Applied Surface Science, 392, 658-686.

Mulewa W., Tahir M., Amin N.A.S., 2017, MMT-supported Ni/TiO_2 nanocomposite for low temperature ethanol steam reforming toward hydrogen production, Chemical Engineering Journal, 326, 956-969.

Reverberi A.P., Klemeš J.J., Varbanov P.S., Fabiano B., 2016, A review on hydrogen production from hydrogen sulphide by chemical and photochemical methods, Journal of Cleaner Production, 136, 72-80.

Tahir B., Tahir M., Amin N.A.S., 2017a, Photocatalytic Carbon Dioxide Reduction to Fuels Over Cu-Loaded g-C_3N_4 Nanocatalyst under Visible Light, Chemical Engineering Transactions, 56, 403-408.

Tahir B., Tahir M., Amin N.A.S., 2017b, Photocatalytic CO_2 Reduction to CO over Fe-loaded TiO_2/Nanoclay Photocatalyst, Chemical Engineering Transactions, 56, 1111-1116.

Tahir M., Tahir B., Amin N.A.S., 2017c, Photocatalytic Reverse Water Gas Shift CO_2 Reduction to CO over Montmorillonite Supported TiO_2 Nanocomposite, Chemical Engineering Transactions, 56, 319-324.

Tahir M., Tahir B., Amin N.A.S., Zakaria Z.Y., 2017d, Photo-induced reduction of CO_2 to CO with hydrogen over plasmonic Ag-NPs/TiO_2 NWs core/shell hetero-junction under UV and visible light, Journal of CO_2 Utilization, 18, 250-260.

Xiong Z., Lei Z., Ma S., Chen X., Gong B., Zhao Y., Zhang J., Zheng C., Wu J.C.S., 2017, Photocatalytic CO_2 reduction over V and W codoped TiO_2 catalyst in an internal-illuminated honeycomb photoreactor under simulated sunlight irradiation, Applied Catalysis B, Environmental, 219, 412-424.

Ye S., Wang R., Wu M.-Z., Yuan Y.-P., 2015, A review on g-C_3N_4 for photocatalytic water splitting and CO_2 reduction, Applied Surface Science, 358, 15-27.